IEEE Access
Multidisciplinary | Rapid Review | Open Access Journal

Received 20 February 2023, accepted 30 March 2023, date of publication 12 April 2023, date of current version 17 April 2023.

Digital Object Identifier 10.1109/ACCESS.2023.3266525

RESEARCH ARTICLE

Development of Internet-Based Distributed Test Platform for Fuel Cell Electric Vehicle Powertrain System With Observer

WENXU NIU[1,2] AND CAIPING LIANG[1]

[1]School of Intelligent Manufacturing and Control Engineering, Shanghai Polytechnic University, Shanghai 201209, China
[2]Deburn (Zhejiang) Power Technology Company Ltd., Jiaxing 314000, China

Corresponding author: Wenxu Niu (jingjingjing2008@outlook.com)

This work was supported in part by the Shanghai Education Development Foundation and the Shanghai Municipal Education Commission through the Chenguang Program under Project C81CG20S001, and in part by the Shanghai Universities Young Teacher Training Funding Program under Project A30DB212103-0202.

ABSTRACT As a new form of test validation, fuel cell and Internet-based distributed test platform has gained increasing attention during the period of dual carbon strategy in China. The reliability of the test platform is an important research direction for the distributed test platform. Under the condition of a large international delay during vehicle powertrain system validation and test, how to predict and optimize the system and how to evaluate the optimization effect becomes a research hotspot. In this paper, on the Internet-based distributed test platform for the fuel cell electric vehicle powertrain system, theoretical and simulation analysis of data transmission and dynamic and economic performance is carried out using observer with large time delay. The analysis found that the observer had an impact on vehicle velocity, fuel cell output power, battery output power and electric motor output torque over the entire test system. In addition, the observer can improve system transparency, which measures the subjective feelings of remote distributed system operators, in the above four indicators and almost has no impact on hydrogen consumption. The results of this study provide a powerful theoretical basis for the optimal design of Internet-based distributed test platforms.

INDEX TERMS Fuel cell, powertrain system, internet-based distributed test platform, observer, transparency, energy measurement.

I. INTRODUCTION

The development of automotive products is becoming increasingly global, and new technologies such as Internet can be used to coordinate development platforms in different regions or in different fields, saving development and testing time and energy. A distributed system is a system in which components are distributed on a networked computer, and communication and action coordination are performed between components by transmitting messages. Nowadays, the degree of globalization of the industrial chain and supply chain of the automobile industry is deepening. To achieve the goal of real-time testing, two or more geographically distributed systems can be connected over an Internet network. Such systems have been applied to enterprises such as Schaeffler and AVL in order to develop a new type of electric site. Unlike the distributed energy system in the energy field, the distributed system here is mainly the automotive powertrain system with geographically distributed components and test benches. In the context of the COVID 19 epidemic, such platforms are of great significance in global product development, testing and validation, and play an important role in the early joint development of products.

Data collection, transmission and processing are one of the core issues for the implementation of global product development, testing and validation platform. The quality of the operation depends on the quality of the data transmission. The quality of the network directly affects the performance

The associate editor coordinating the review of this manuscript and approving it for publication was Huaqing Li.

of the test platforms. In addition, the signals transmitted between regions are electric signal instead of actual energy. Although some work considers and uses information data and physical data at the same time, which can make up for the above deficiencies to a certain extent, but in the actual implementation process, the two kinds of data are often isolated, lacking comprehensive interaction and In-depth fusion, the consistency and synchronization of information and physics are poor, and the real-time and accuracy of the results need to be improved. It is unknown how this transmission method effects the local energy signals, how this transmission method effects on dynamic and economic performance in powertrain system test and validation, and how the affects will be if some improvement methods are carried out. Therefore, how to improve cross-regional data transmission and measure the improved effect, especially the characteristics of energy signals, is an urgent problem to be solved.

In recent years, several research institutions and companies have studied this kind of system and have proposed some validation and optimization methods. Based on the traditional network model-based predictive control scheme (NMBPC), Rahmani et al. proposed the Plant Input Mapping (PIM) discretization technique to ensure the closed-loop stability performance [1]. The controller on one side produces a series of stable control outputs, each associated with a predetermined network time delay; the other side of the delay compensator receives the output signal from the controller with a certain delay and then selects from the range matching the delay appropriate control outputs, to complete the control process. Another method to overcome the delay stability problem of NMBPC is based on the event method, namely, the variables selecting control (VSC). In this method, the system output on one side is executed only when a new input signal from the controller on the other side is received. To achieve closed-loop control, the appropriate discrete-time model must be calculated offline. The VSC method has been shown to have a tolerance for relatively large network delays and packet loss [2], [3]. Fractional-order controllers are now widely used in network control systems with the advantage of large jitter margins [4]. The jitter margin is how much additional delay the system tolerates to maintain a stable indicator [5]. Bhambhani et al. implemented an optimal fractional-order PI (OFOPI) controller into a network control system called ''smart wheel'', which is an automatic wheel that is remotely controlled over the Internet [6]. Neural network is globally optimized to effectively predict and compensate for the time delay in data transmission. However, this method requires a large amount of data for offline neural network training, and the optimization effect depends on the training data. Because the actual state of the network connection is deviated from the training data, the prediction compensation based on neural network has limitations. The observer method was carried out considering the bilateral system, however this bilateral system is in a small delay system condition [7]. In response to the delay of combination tests of some software and hardware on-road, fuzzy control methods were adopted to manage and balance the torque signals between the software and hardware [8]. A novel approach was proposed for the simultaneous identification of vehicle model parameters and road profile, utilizing the availability of fleet data, The approach exploited a low-order model in which the parameters were identified for a specific asset (i.e., a digital twin) [9]. A novel performance optimization framework based on deep-reinforcement learning was proposed for Internet of vehicles, where transactional throughput was maximized while guaranteeing decentralization, latency, and security of the underlying block chain system [10].

The distributed system validation control theory method mentioned in the above literature is beneficial to the layout and optimization of distributed systems, and has a certain isolation effect on the factors affecting the performance of distributed systems, but the above methods are mainly aimed at delays less than 100ms. The situation, for the application of large delays, needs to be discussed.

For the issue of energy signal transmission, most current research is centered on distributed energy systems and IoT-based microsystems. For distributed energy systems, its main research areas are power and energy conversion, intelligent control and group control optimization technology. The recent rapid development of communication technologies in telemetry and remote control, e.g., smart meters, has established the foundation of Real-time electricity markets' (RTM) implementation [11], [12]. Some research examines whether combinations of renewable distributed generation can make better use of the capacity of the distribution network [13]. For IoT-based microsystems, the main focus is to design and implement a high-precision, high-dynamic range, low-power, and flexible power measurement system, which can be applied to different applications [14]. The working condition and arrangement of automotive powertrain system are different from that of a distributed energy system. The power level of the automotive powertrain system is much larger than that of the IoT-based microsystem. Therefore, for the issue of transmission of energy signals, there is no relevant literature to study the transmission of energy signals at this power level.

Therefore, the main purpose of this paper is to use the observer to establish a distributed test platform optimization method for the fuel cell vehicle powertrain under the condition of a large time delay, and to validate the signal, especially the transmission effect of the energy signal. In this paper, an Internet-based distributed test platform for fuel cell electric vehicle powertrain system is built with an observer in Section II, in order to estimate and contrast the influence of large delay (more than 100ms). In Section III, an optimizing data transmission method with observer and how this transmission method affects dynamic performance are discussed. In Section IV, data transparency analysis is performed to validate any impact on system performance. In Section V, how this transmission method affects economic performance is discussed with the help of transparency analysis.

II. SYSTEM MODEL

A. DISTRIBUTED TEST PLATFORM

According to the needs for joint research and development of fuel cell powertrain system between two distant places, a distributed test platform of fuel cell electric vehicle powertrain system is established. The research contents include calculation of the energy consumption of the powertrain system, as well as validating fuel economy of the powertrain system. Another goal is to remotely connect the developed environment of the distributed platform's and realize the data transfer capability between two long-delay places. In the actual measurement, it is found that the time delay between two places is more than 100ms, so the main purpose of this paper is to explore the system optimization under the condition of large time delay. This paper uses the powertrain system and various component models in the platform mentioned above, and the time delay condition simulates the large time delay in the measurement.

B. CONFIGURATION OF FUEL CELL MODEL

One of the power sources in this powertrain system is the fuel cell. Proton exchange membrane fuel cell (PEMFC), with its high energy conversion efficiency, very low pollutant emissions, and flexibility, is known as one of the most promising power generation technologies [19], [20]. The working principle of PEMFC is through electrochemical reactions that use hydrogen and oxygen to generate electrical energy [21], [22]. In fact, the complexity of the fuel cell subsystem also enables the dynamic response of the fuel cell to become worse, and subject to a greater influence of the surrounding work environment. Currently, [23] and [24] help making a simplified model. In order to more accurately describe the fuel cell system, and the parameter identification data are fit to improve the accuracy of the simplified model and make it easy to understand the common method. When the load current changes, since the surface of the charging effect of the bipolar plate, the fuel cell will produce slowly varying voltage. The equivalent resistor Ra and the capacitor C are connected in parallel. The efficiency of the fuel cell system is calculated using Equation (1) [25].

$$\eta_{FC} = \frac{U_{FC} l_{FC}}{m_{H_2} LHV_{H_2}} \times 100\% \tag{1}$$

where η_{FC} is the efficiency of the fuel cell system, U_{FC} is the voltage of the fuel cell system, l_{FC} is the current of the fuel cell system, m_{H_2} is the mass flow of hydrogen and LHV_{H_2} is the low heating value of hydrogen, $1.2 \times 10\text{^}5$ kJ/kg. η_{FC}, U_{FC}, l_{FC} and m_{H_2} were evaluated by preliminary test. The values of single fuel cells and the power values of the fuel cell are shown in Table 2.

C. BATTERY PARAMETERS

The battery can compensate for the lack of dynamic response of the fuel cell and absorb the energy of the brake [26], [27]. Here a packaged ternary polymer lithium battery model is used. The battery and fuel cell are connected in parallel, using a power following strategy. In this paper, the analytic model of the battery will be used. The input is the battery current and temperature, and the output is the voltage and state of charge (SOC). By stationary state the charging mode of our vehicle is constant current-constant voltage cycle. For this battery model, the following assumptions exist: the internal resistance of the battery model is constant, that is, the internal resistance value is kept constant during the charging and discharging process of the battery, and is also independent of the charge and discharge current; there is no memory effect in the battery. The battery model is mainly divided into three modules: SOC calculation module, voltage calculation module, and a thermal calculation module. The maximum capacity of the battery is related to the temperature. The battery value is shown in Table 3. The battery model parameters and test data are provided by AVL.

TABLE 1. Vehicle key parameters [17], [18].

Name	Parameter	Unit
Vehicle weight	1600	kg
Transmission ratio	1	-
Transmission system efficiency	92	%
Tire radius	0.3	m
Rolling resistance coefficient	0.01	-
Air resistance coefficient	0.35	-
Frontal area	2.8	m2
10 °C sea level air density	1.2	N·s2·m-4
Rotational mass conversion factor	1.05	-
Drive torque	-	N·m
Vertical speed	-	m/s
Vertical acceleration	-	m/s2

TABLE 2. Fuel cell values [21].

Name	Value	Unit
Single internal resistance	0.0003	Ω
Single equivalent resistance	0.0006	Ω
Single open circuit voltage	1.037	V
Single equivalent capacitor	3	F
Fuel cell rated power	6	kW
Fuel cell peak power	6.5	kW

D. ELECTRIC MOTOR PARAMETERS

The transmission system contains four in-wheel motors. The motor model is a quasi-steady state model [28]. The motor parameters are shown in Table 4.

III. STUDY ON OPTIMIZING DATA TRANSMISSION METHOD WITH OBSERVER

A. OBSERVER DESIGN

Since there is a nonlinear part on both sides of the distributed test platform, it is difficult to directly measure control input

TABLE 3. Battery values [21].

Name	Value	Unit
Maximum current	500	A
Maximum charging current	−45	A
Number of batteries in series	100	-
Number of batteries in parallel	20	-
Cell radius	0.013	m
Battery height	0.065	m
Battery capacity	2.3 × 3600	Ah·s
C rate (charge and discharge current/rated capacity)	1	C

TABLE 4. Electric motor parameters [21].

Name	Value	Unit
Drive Type	4 In-Wheel Motor	–
In-Wheel Motor Rated/Peak Power	4 × 0.8/4 × 2.5	kW

and disturbance, and it is necessary to construct a system to realize state estimation of the original system. The system used to estimate the state of the original system is called a state estimator or a state observer [10].

Let a single input nonlinear system be defined as

$$x^{(n)} = f(\mathbf{x}, t) + b(\mathbf{x}, t)\, u(t) \tag{2}$$

Here $\mathbf{x}(t)$ is the state vector, $u(t)$ is the control input, x is the output state of the interest. The error value is

$$\tilde{\mathbf{x}}(t) = \mathbf{x}(t) - \mathbf{x_d}(t) = \left[\tilde{x}(t)\ \dot{\tilde{x}}(t)\ \cdots\ \tilde{x}^{(n-1)}(t)\right]^T \tag{3}$$

Here $\mathbf{x}_d$ is remote subsystem state variable. If $n = 2$, here

$$\begin{cases} \tilde{x}_1(t) = x_{1d}(t) - x_1(t) \\ \tilde{x}_2(t) = x_{2d}(t) - x_2(t) \end{cases} \tag{4}$$

Furthermore, the time varying surface $s(t)$ in the state-space $\mathbf{R}^{(n)}$ by the scalar equation $s(\mathbf{x}; t) = 0$.Here the sliding mode observer is first defined by the sliding surface equation

$$s(\mathbf{x}; t) = \left(\frac{d}{dt} + \lambda\right)^{n-1} \tilde{x} = 0 \tag{5}$$

Here λ is design parameter. If the system is to be held on a sliding surface with $n = 2$, it must be satisfied

$$\dot{x}(t) = \dot{x}_d(t) - \lambda\,(x(t) - x_d(t)) \tag{6}$$

Bounds on s can be directly translated into bounds on the tracking error vector $\tilde{\mathbf{x}}$; therefore, the scalar s represents a true measure of tracking performance. The corresponding transformations of performance measures assuming $\tilde{x}(0) = 0$ is

$$\forall t \geq 0, |s(t)| \leq \phi \ \Rightarrow\ \forall t \geq 0, \left|\tilde{x}^{(i)}(t)\right| \leq (2\delta)^i \varepsilon \quad i = 0, \cdots, n-1 \tag{7}$$

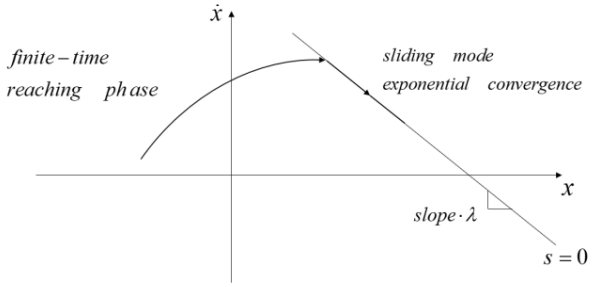

FIGURE 1. Graphical interpretation of Equation (5) and Equation (8).

where $\varepsilon = \phi/\delta^{n-1}$ [29]. In order to keep s at zero by choosing control law of Equation (2)

$$\frac{1}{2} \cdot \frac{d}{dt} s^2 \leq -\eta\,|s| \tag{8}$$

Here η is a strictly positive constant. Equation (8) states that the squared "distance" to the surface, as measured by s^2, decreases along all system trajectories. The satisfaction of condition (8), or the sliding condition, makes the surface an invariant set.

The typical system behavior implied by satisfying sliding condition Equation (8) is illustrated in Figure 1 for $n = 2$. The sliding surface is a line in the phase plane, of slope - λ and containing the time-varying point $\mathbf{x}_d = \left[x_d\ \dot{x}_d\right]^T$. Starting from any initial condition, the state trajectory reaches the time-varying surface in a finite time smaller than $|s(t=0)|/\eta$, and then slides along the surface towards $\mathbf{x}_d = \left[x_d\ \dot{x}_d\right]^T$ exponentially, with a time-constant equal to $1/\lambda$. Different values of λ correspond to different rates of reaching the sliding surface.

According to Equation (5), if $\mathbf{x}(t=0)$ is actually off $\mathbf{x}_d(t=0)$, the surface will nonetheless be reached in a finite time smaller than $|s(t=0)|/\eta$. Assume that $s(t=0) > 0$, t_{reach} means the time to hit the surface $s = 0$. Therefore Equation (8) between $t = 0$ and $t = t_{reach}$ leads to

$$0 - s(t=0) = s(t = t_{reach}) - s(t=0) \leq -\eta\,(t_{reach} - 0) \tag{9}$$

Therefore,

$$t_{reach} \leq s(t=0)/\eta \tag{10}$$

The same result as with $s(t=0) < 0$. Equation (5) implies that, once on the surface, the tracking error tends to zero with a time constant $(n-1)/\lambda$.

The distributed system architecture with Internet latency and state observers is shown in Figure 2. Here, Subsystem 1 runs working condition information, driver model, ECU model, fuel cell system model and battery model; Subsystem 2 runs E-motor model and vehicle dynamics model. On the distributed test platform, Subsystem 1 runs in place 1 and Subsystem 2 runs in place 2. According to the energy flow, subsystem 1 acts as the server and subsystem

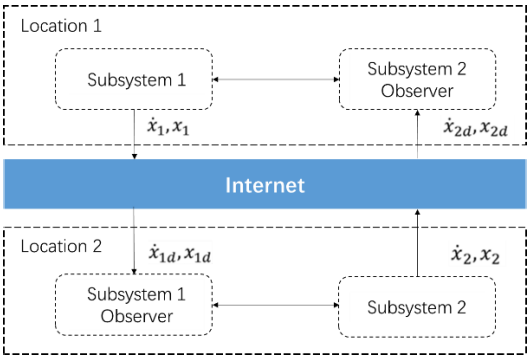

FIGURE 2. System structure with observer.

2 acts as the client. In order to verify the performance of the observer in this paper, both Subsystem 1 and Subsystem 2 run in place 1, and the actual network delay time is replaced by the simulation delay time.

Rewrite (3) to the following form, Subscript d means delayed variable

$$\begin{aligned}\dot{\tilde{x}}(t) &= \dot{x}(t) - \dot{x}_d(t) \\ &= \dot{x}_d(t-t_d) - \lambda\left(x(t-t_d) - x_d(t-t_d)\right) - \dot{x}_d(t) \\ &= \dot{x}_d(t-t_d) - \lambda\tilde{x}(t-t_d) - \dot{x}_d(t) \\ &= -\lambda\tilde{x}(t-t_d) + w \end{aligned} \tag{11}$$

Here

$$w = \dot{x}_d(t-t_d) - \dot{x}_d(t) \tag{12}$$

The stability of Equation (12) is determined by (13)

$$\begin{aligned} s + \lambda e^{-st_d} &= 0 \\ s &= \frac{W\left(-\lambda t_d\right)}{t_d} \end{aligned} \tag{13}$$

$$\lambda < \frac{\pi}{2t_d} \tag{14}$$

Here W is Lambert W function, λ shall satisfy Equation (14) to satisfy the stability conditions of the system [30]. According to Equation (13), λ can be selected as a function of t_d to ensure the asymptotic stability of the error system even for non-zero time delays. Therefore, even though the error system will not strictly stay on the sliding surface would, it will still converge to zero. This means that there is no need for any further control action to drive the error system to the sliding surface. On this basis, a series of λ values that meet the requirements should be selected to verify the influence of different sliding surfaces on the system.For subsystem 1, the state observer equation is as shown in Equation (15)

$$\begin{aligned}\dot{x}_1(t) &= \dot{x}_{1d}(t-t_{d2}) - \lambda\left(x_1(t-t_{d2}) - x_{1d}(t-t_{d2})\right) \\ \dot{x}_2(t) &= \dot{x}_{2d}(t-t_{d2}) - \lambda\left(x_2(t-t_{d2}) - x_{2d}(t-t_{d2})\right)\end{aligned} \tag{15}$$

Here x_1 is actual output power p_{ist} of power sources, x_2 is demand torque T_{soll} of E-motor.

For subsystem 2, the state observer equation is as shown in Equation (16)

$$\begin{aligned}\dot{x}_3(t) &= \dot{x}_{3d}(t-t_{d1}) - \lambda\left(x_3(t-t_{d1}) - x_{3d}(t-t_{d1})\right) \\ \dot{x}_4(t) &= \dot{x}_{4d}(t-t_{d1}) - \lambda\left(x_4(t-t_{d1}) - x_{4d}(t-t_{d1})\right)\end{aligned} \tag{16}$$

Here x_3 is actual velocity v_{act} of ECU, x_4 is demand power p_{req} of power sources.

The performance of the norm value of the difference between the observed value and the standard value is characterized according to the literature [31]. Assume

$$p = \|v - v_i\|_2 \tag{17}$$

$$p_n = \frac{\|v - v_i\|_2}{\|v_d - v_i\|_2} \tag{18}$$

Here p is performance indicator, p_n is performance indicator after normalized processing p, v is observation indicator, v_i is no standard observer without delay indicator, v_d is no standard observer with delay indicator. $p = p_n = 0$ is ideal state, in this case, it is completely unaffected by the delay. When $p_n > 1$, the observer has an adverse effect on the optimization of performance indicator; when $p_n < 1$, the observer has a positive effect on the optimization of performance indicator.

B. INFLUENCE OF SYSTEM WITH OBSERVER

In order to validate the effect of the observer on the performance of the system, the system is simulated with a one-way delay of 250ms, 400ms, and 500ms. According to [28], 250ms and 400ms are the more frequent delays, and 500ms is the dividing line between delay and packet loss. In [28] the analysis found that data loss had an impact on vehicle speed over the entire test system. Especially when the data packet loss rate exceeded 5%, the impact on system stability could not be ignored. Based on this research, a robust model predictive compensator with state compensation was designed. Under the action of the predictive compensator, its optimization ability for the Internet-based distributed test platform was validated by simulation analysis. RMPC (Robust Model Predictive Control) effectively improved the stability of the system. Compared with the Internet-based distributed test platform without the predictive compensator, it greatly improved the system performance of the Internet-based distributed test platform. This method has been applied in the basic network configuration of this paper to eliminate the impact of packet loss to the maximum extent.

Therefore, these three delay values are selected. The driving cycle is WLTP. Set $\lambda = 0.5, \lambda = 1, \lambda = 1.5$, when the one-way delay is 250ms (round-trip delay is 500ms), the simulation results of speed, fuel cell output power, battery output power and motor torque are shown in Figure 3, Figure 4, Figure 5, and Figure 6. In order to better display the results, here select the 600-800 seconds of WLTP working conditions.

As can be seen from Figure 3, Figure 4, Figure 5, and Figure 6, when the one-way delay is 250ms (the round trip

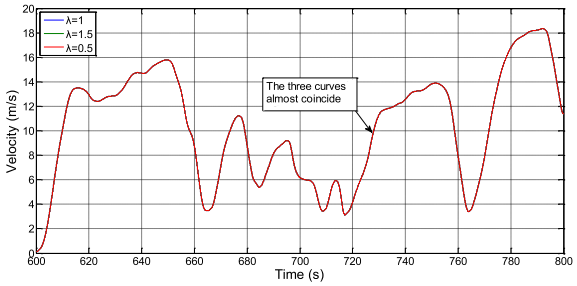

FIGURE 3. Velocity simulation result of 250ms one-way delay.

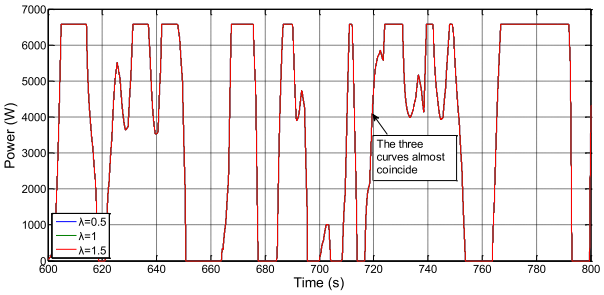

FIGURE 4. Fuel cell output power simulation result of 250ms one-way delay.

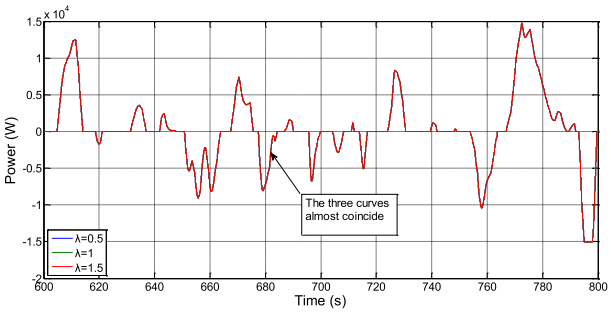

FIGURE 5. Battery output power simulation result of 250ms one-way delay.

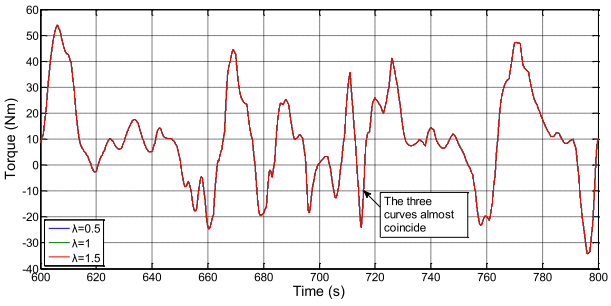

FIGURE 6. Electric motor output torque simulation result of 250ms one-way delay.

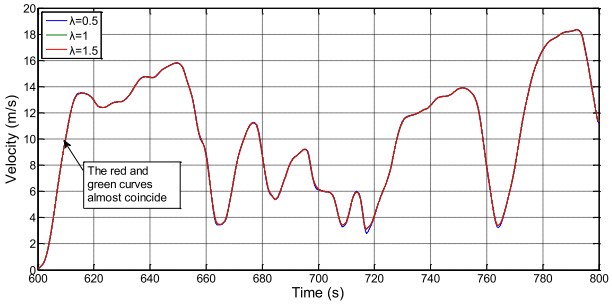

FIGURE 7. Velocity simulation result of 400ms one-way delay.

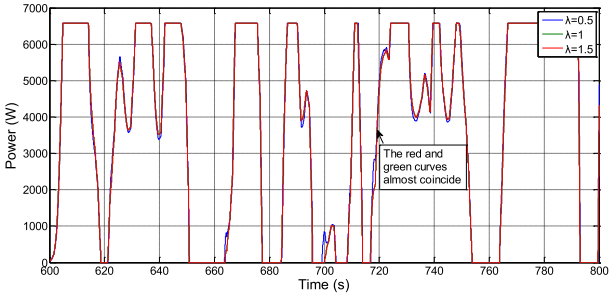

FIGURE 8. Fuel cell output power simulation result of 400ms one-way delay.

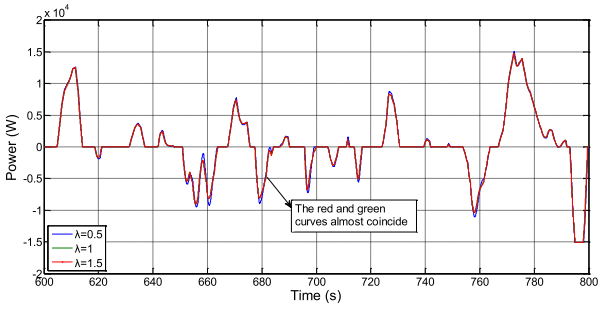

FIGURE 9. Battery output power simulation result of 400ms one-way delay.

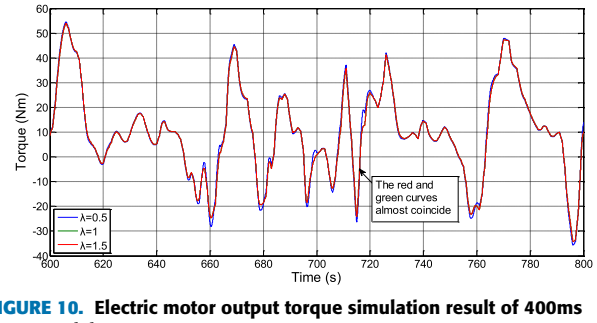

FIGURE 10. Electric motor output torque simulation result of 400ms one-way delay.

delay is 500ms), no matter what the value of λ is, the optimization effect is almost the same on several indicators.

When the one-way delay is 400ms (the round trip delay is 800ms), the simulation results of velocity, fuel cell output power, battery output power, and electric motor output torque are shown in Figure 7, Figure 8, Figure 9, and Figure 10.

As can be seen from Figure 7, Figure 8, Figure 9, and Figure 10, when the one-way delay is 400ms (the round trip delay is 800ms), the optimization effect of $\lambda = 0.5$ is significantly different with $\lambda = 1$ and $\lambda = 1.5$.

When the one-way delay is 500ms (the round trip delay is 1000ms), the simulation results of velocity, fuel cell output power, battery output power, and electric motor output torque are shown in Figure 11, Figure 12, Figure 13, and Figure 14.

As can be seen in Figure 11, Figure 12, Figure 13, and Figure 14, when the one-way delay is 500ms (round trip delay is 1000ms), there is no significant difference in the

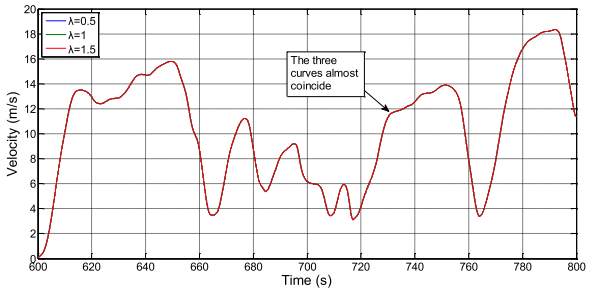

FIGURE 11. Velocity simulation result of 500ms one-way delay.

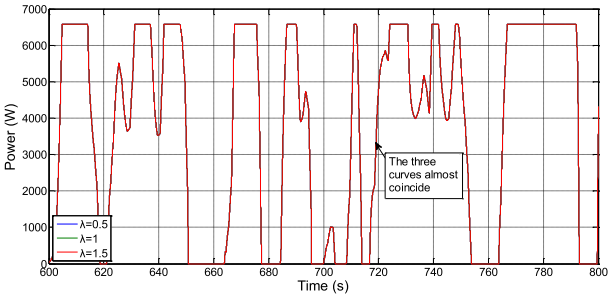

FIGURE 12. Fuel cell output power simulation result of 500ms one-way delay.

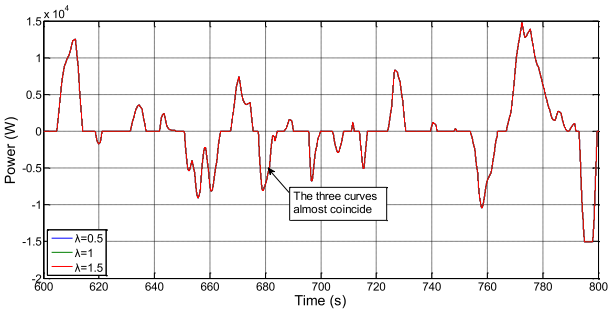

FIGURE 13. Battery output power simulation result of 500ms one-way delay.

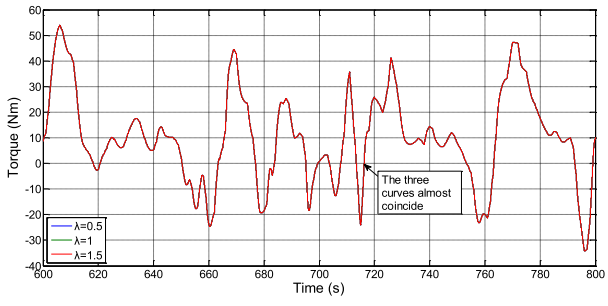

FIGURE 14. Electric motor output torque simulation result of 500ms one-way delay.

optimization of several performance indicators for different values of λ.

Therefore, from Figure 3 to Figure 14, some rules can be obtained on the effect of the observer on performance. In order to further illustrate the effect of the observer, the values λ of the velocity, fuel cell output power, battery output power, electric motor output torque for different delay are calculated as performance indicators, as shown in Table 5, Table 6, Table 7, Table 8.

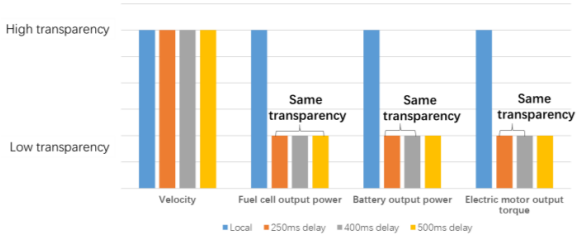

FIGURE 15. Comparison of different parameter transparency.

TABLE 5. Comparison of velocity performance indicators.

	250ms	400ms	500ms
$\lambda = 0.5$	0.99	0.61	0.28
$\lambda = 1$	0.99	1.00	0.28
$\lambda = 1.5$	0.99	0.99	0.28

TABLE 6. Comparison of fuel cell output power performance indicators.

	250ms	400ms	500ms
$\lambda = 0.5$	1.00	0.62	0.33
$\lambda = 1$	1.00	1.00	0.33
$\lambda = 1.5$	1.00	1.00	0.33

TABLE 7. Comparison of battery output power performance indicators.

	250ms	400ms	500ms
$\lambda = 0.5$	1.00	0.67	0.37
$\lambda = 1$	1.00	1.00	0.37
$\lambda = 1.5$	1.00	1.00	0.37

TABLE 8. Comparison of electric motor output torque performance indicators.

	250ms	400ms	500ms
$\lambda = 0.5$	1.00	0.61	0.28
$\lambda = 1$	1.00	1.00	0.28
$\lambda = 1.5$	1.00	1.00	0.28

From Table 5, when the one-way delay is 250ms, regardless of the value of λ, the optimization effect on the velocity is consistent, and there is no obvious optimization effect. When the one-way delay is 400ms, the corresponding $\lambda = 0.5$ velocity performance indicator is 0.61, which is better than $\lambda = 1$ and $\lambda = 1.5$. When the one-way delay is 500ms, regardless of the value of λ, the optimization effect on the velocity is consistent. The performance indicators are 0.28, and the optimization effect is obvious.

From Table 6, when the one-way delay is 250ms, regardless of the value of λ, the optimization effect on the fuel cell output power is consistent, and there is no obvious optimization effect. When the one-way delay is 400ms, the corresponding $\lambda = 0.5$ fuel cell output power performance indicator is 0.62, which is better than $\lambda = 1$ and $\lambda = 1.5$.

When the one-way delay is 500ms, regardless of the value of λ, the optimization effect on the fuel cell output power is consistent. The performance indicators are 0.33, and the optimization effect is obvious.

From Table 7, when the one-way delay is 250ms, regardless of the value of λ, the optimization effect on the battery output power is consistent, and there is no obvious optimization effect. When the one-way delay is 400ms, the corresponding $\lambda = 0.5$ battery output power performance indicator is 0.67, which is better than $\lambda = 1$ and $\lambda = 1.5$. When the one-way delay is 500ms, regardless of the value of λ, the optimization effect on the battery output power is consistent. The performance indicators are 0.37, and the optimization effect is obvious.

From Table 8, when the one-way delay is 250ms, regardless of the value of λ, the optimization effect on the electric motor output torque is consistent, and there is no obvious optimization effect. When the one-way delay is 400ms, the corresponding $\lambda = 0.5$ electric motor output torque performance indicator is 0.61, which is better than $\lambda = 1$ and $\lambda = 1.5$. When the one-way delay is 500ms, regardless of the value of λ, the optimization effect on the electric motor output torque is consistent. The performance indicators are 0.28, and the optimization effect is obvious.

It can be seen from the above analysis that when $\lambda = 0.5$, the optimization effect on fuel cell output power, battery output power and electric motor output torque is most obvious. This means that in terms of dynamic performance, the introduction of observer can better achieve dynamic performance improvement under large delay conditions. This conclusion is of great significance for the dynamic performance test and validation of powertrain systems on such platforms.

IV. OBSERVER IMPACT ON TRANSPARENCY

The concept of transparency is mainly used to measure the difference between teleoperation and non-teleoperation. In this way, it is an important indicator of transmission efficiency. In order to evaluate the transparency of different configurations, a statistical analysis method should be considered, preferably a non-parametric analysis method. Non-parametric analysis (also known as free test distribution) is mainly used to solve the overall distribution of unknown statistical inference, and can complete lower-level inferred measurement data. The Kruskal-Wallis test is a non-parametric test method, which determines whether the distribution of p-values is the same by observing the values in multiple independent population samples. The p value can be determined by the lookup table [28]. According to this method, the above-mentioned data including vehicle speed, fuel cell power, battery power and motor torque are processed.

Therefore, for systems with $\lambda = 0.5$ observer, the transparency of velocity, fuel cell output power, battery output power, and electric motor output torque must be calculated as shown in Table 9, Table 10, Table 11, and Table 12. ''Significant'' in Table 9, Table 10, Table 11, and Table 12 is the p-value. According to the definition of p-value, it can be considered that when $p > 0.05$, the indicators compared have the same transparency.

TABLE 9. Pairwise comparison of velocity parameters.

Sample 1 - Sample 2	Average difference	Standard deviation	Significant
0ms-250ms	0.00092	0.03336	1.000
0ms-250ms with observer	0.00084	0.03336	1.000
0ms-400ms with observer	0.00091	0.03336	1.000
0ms-500ms with observer	0.00084	0.03336	1.000
250ms-250ms with observer	-0.00008	0.03336	1.000
250ms-400ms with observer	-0.00001	0.03336	1.000
250ms-500ms with observer	-0.00008	0.03336	1.000

TABLE 10. Pairwise comparison of fuel cell output power parameters.

Sample 1 - Sample 2	Average difference	Standard deviation	Significant
0ms-250ms	-38.10518	9.96030	0.001
0ms-250ms with observer	-38.18946	9.96030	0.001
0ms-400ms with observer	-57.71245	9.96030	0.000
0ms-500ms with observer	-38.18946	9.96030	0.001
250ms-250ms with observer	-0.08428	9.96030	1.000
250ms-400ms with observer	-19.60727	9.96030	0.281
250ms-500ms with observer	-0.08428	9.96030	1.000

For the velocity parameter, regardless of the presence or absence of the observer, the velocity is highly transparent compared to the no-delay state, and the observer has no effect on the transparency. For fuel cell output power, although the observer is increased, the delay remains low transparency compared to no delay, but it is worth noting that when comparing the 400ms, 500ms one-way delay with the observer and the 250ms delay, the transparency is the same, and it can be considered that the observer has a positive effect on the improvement of the transparency of the system in this case. Similarly, for battery output power and electric motor output torque, the transparency of the 400ms one-way delay with the observer is consistent with the transparency at 250ms delay, which also reflects the positive effect of the observer on the transparency of the system. The transparency of the different parameters is shown in Figure 15. When the p-value

TABLE 11. Pairwise comparison of battery output power parameters.

Sample 1 - Sample 2	Average difference	Standard deviation	Significant
0ms-250ms	-38.10518	13.72589	0.044
0ms-250ms with observer	-38.18946	13.72589	0.043
0ms-400ms with observer	-38.18946	13.72589	0.043
0ms-500ms with observer	1014.42250	13.72589	0.000
250ms-250ms with observer	-0.08428	13.72589	1.000
250ms-400ms with observer	-0.08428	13.72589	1.000
250ms-500ms with observer	1052.52768	13.72589	0.000

TABLE 12. Pairwise comparison of electric motor output torque parameters.

Sample 1 - Sample 2	Average difference	Standard deviation	Significant
0ms-250ms	-0.18953	0.04823	0.001
0ms-250ms with observer	-0.19401	0.04823	0.001
0ms-400ms with observer	-0.27733	0.04823	0.000
0ms-500ms with observer	-0.94083	0.04823	0.000
250ms-250ms with observer	-0.00448	0.04823	1.000
250ms-400ms with observer	-0.08780	0.04823	0.362
250ms-500ms with observer	-0.75130	0.04823	0.000

of the a 'certain' delay (e.g. 250ms) and zero delay is greater than 0.05, that means the transparency of the two groups is the same, i.e. high transparency. When the p-value of the a 'certain' delay (e.g. 500ms) and the zero delay is smaller than 0.05, that means that the transparency of the two groups is not the same, i.e. low transparency.

For the distributed test platform for the fuel cell electric vehicle powertrain system, the observer used in this paper can effectively reduce the negative impact due to network delay.

V. OBSERVER IMPACT ON ENERGY MEASUREMENT SIMULATION

Besides the observer impacts on delay prediction and transparency, whether energy measurements of validation and test process would be influenced by observer, is another issue worthy of attention. Here, hydrogen consumption, fuel cell output energy and battery output energy in the model are simulated, as shown in Table 13-Table 15.

TABLE 13. Hydrogen consumption with different λ (gal).

	250ms	400ms	500ms
No observer	1.1392	1.1602	1.1728
$\lambda = 0.5$	1.1392	1.1454	1.1728
$\lambda = 1$	1.1392	1.1602	1.1728
$\lambda = 1.5$	1.1392	1.1602	1.1728

TABLE 14. Fuel cell output energy (kJ).

	250ms	400ms	500ms
No observer	6115.9	6234.8	6303.1
$\lambda = 0.5$	6116.1	6151.2	6116.1
$\lambda = 1$	6116.0	6116.0	6116.0
$\lambda = 1.5$	6116.0	6116.0	6116.0

TABLE 15. Battery output energy (kJ).

	250ms	400ms	500ms
No observer	4221.0	4241.5	4136.0
$\lambda = 0.5$	4221.0	4221.4	4221.0
$\lambda = 1$	4221.0	4221.0	4221.0
$\lambda = 1.5$	4221.0	4221.0	4221.0

In Table 13, it is worth noting that, at the same time delay, the hydrogen consumption is nearly the same regardless of the value of λ. As the delay increases, the hydrogen consumption also increases because the presence of the delay extends the start-up time of the fuel cell.

From Table 14-Table 15, in the absence of the observer, as the time delay increases, the output energy of the fuel cell increases and the output energy of the battery decreases. The energy here is all effective energy, which is used to drive vehicle. The total amount of energy in the fuel cell and battery is fixed because of the certain working condition.

Under the action of the observer, the energy distribution of the fuel cell and the battery under long-term delay conditions is close to the short delay conditions under the indicator of transparency. This is the result of the observer significantly improving transparency of the whole system. This conclusion is of great significance for the economic performance test and validation of powertrain systems on such platforms. In the future, different time delays and different λ will also be considered for the safety of the entire platform and the characteristics of the components.

VI. CONCLUSION

In this paper, the theoretical and simulation analysis of data transmission using an observer with a large time delay for an Internet-based distributed test platform was carried out. The analysis found that the observer had an impact on signal exchange of vehicle velocity, fuel cell output power, battery output power and electric motor output torque over the entire test system. Especially when $\lambda = 0.5$, the observer

optimization effect on fuel cell output power, battery output power and electric motor output torque is most obvious. With the help of nonparametric statistics, the transparency in fuel cell output power, battery output power and electric motor output torque in the structure with the observer has been improved. Under the action of the observer, the energy distribution of the fuel cell and the battery under long-term delay conditions is close to the short delay condition.

REFERENCES

[1] B. Rahmani, P. M. Nezhad, and A. H. D. Markazi, "Plant input-mapping-based predictive control of systems through band-limited networks," *IET Control Theory Appl.*, vol. 5, no. 2, pp. 341–350, Jan. 2011.

[2] B. Rahmani and A. H. D. Markazi, "Variable selective control method for networked control systems," *IEEE Trans. Control Syst. Technol.*, vol. 21, no. 3, pp. 975–982, May 2013.

[3] B. Rahmani, A. H. Markazi, and B. Seyfi, "A new method for control of networked systems with an experimental validation," *ISA Trans.*, vol. 56, pp. 299–307, May 2015.

[4] V. Bhambhani, Y. Chen, and D. Xue, "Optimal fractional order proportional integral controller for varying time-delay systems," *IFAC Proc. Volumes*, vol. 41, no. 2, pp. 4910–4915, 2008.

[5] A. Cervin, B. Lincoln, J. Eker, R. Karl-Erik, and G. Buttazzo, "The jitter margin and its application in the design of real-time control systems," in *Proc. 10th Int. Conf. Real-Time Embedded Comput. Syst. Appl.*, Goteborg, Sweden, 2004, pp. 1–10.

[6] V. Bhambhani, Y. Han, S. Mukhopadhyay, Y. Luo, and Y. Chen, "Random delay effect minimization on a hardware-in-the-loop networked control system using optimal fractional order PI controllers," in *Proc. 3rd IFAC Workshop Fractional Differentiation Appl.*, Ankara, Turkey, 2008, pp. 1–6.

[7] A. Tandon, M. J. Brudnak, J. L. Stein, and T. Ersal, "An observer based framework to improve fidelity in internet-distributed hardware-in-the-loop simulations," in *Proc. ASME Dyn. Syst. Control Conf.*, Palo Alto, CA, USA, 2013, p. 3878.

[8] Y. Zhang, S. Lu, Y. Yang, and Q. Guo, "Internet-distributed vehicle-in-the-loop simulation for HEVs," *IEEE Trans. Veh. Technol.*, vol. 67, no. 5, pp. 3729–3739, May 2018.

[9] F. Naets, J. Geysen, and W. Desmet, "An approach for combined vertical vehicle model and road profile identification from heterogeneous fleet data," in *Proc. IEEE Int. Conf. Connected Vehicles Expo (ICCVE)*, Graz, Austria, Nov. 2019, pp. 1–5.

[10] M. Liu, Y. Teng, F. R. Yu, V. C. M. Leung, and M. Song, "Deep reinforcement learning based performance optimization in blockchain-enabled Internet of Vehicle," in *Proc. IEEE Int. Conf. Commun. (ICC)*, Shanghai, China, May 2019, pp. 1–6.

[11] Q. Wang, C. Zhang, Y. Ding, G. Xydis, J. Wang, and J. Østergaard, "Review of real-time electricity markets for integrating distributed energy resources and demand response," *Appl. Energy*, vol. 138, pp. 695–706, Jan. 2015.

[12] A. J. Conejo, J. M. Morales, and L. Baringo, "Real-time demand response model," *IEEE Trans. Smart Grid*, vol. 1, no. 3, pp. 236–242, Dec. 2010.

[13] W. Sun and G. P. Harrison, "Wind-solar complementarity and effective use of distribution network capacity," *Appl. Energy*, vol. 247, pp. 89–101, Aug. 2019.

[14] Y. H. Tehrani and S. M. Atarodi, "Design & implementation of a high precision & high dynamic range power consumption measurement system for smart energy IoT applications," *Measurement*, vol. 146, pp. 458–466, Nov. 2019.

[15] H. Gao, T. Zhang, H. Chen, Z. Zhao, and K. Song, "Application of the X-in-the-loop testing method in the FCV hybrid degree test," *Energies*, vol. 11, no. 2, p. 433, Feb. 2018.

[16] M. Abe, *Vehicle Handling Dynamics: Theory and Application*. Oxford, U.K.: Butterworth-Heinemann, 2015.

[17] S. Ke, F. Li, X. Hu, L. He, W. Niu, S. Lu, and T. Zhang, "Multi-mode energy management strategy for fuel cell electric vehicles based on driving pattern identification using learning vector quantization neural network algorithm," *J. Power Sources*, vol. 389, pp. 230–239, Jun. 2018.

[18] W. Niu, K. Song, Q. Xiao, M. Behrendt, A. Albers, and T. Zhang, "Transparency of a geographically distributed test platform for fuel cell electric vehicle powertrain systems based on X-in-the-loop approach," *Energies*, vol. 11, no. 9, p. 2411, Sep. 2018.

[19] Y. Wang, H. Xu, X. Wang, Y. Gao, X. Su, Y. Qin, and L. Xing, "Multi-sub-inlets at cathode flow-field plate for current density homogenization and enhancement of PEM fuel cells in low relative humidity," *Energy Convers. Manag.*, vol. 252, Jan. 2022, Art. no. 115069.

[20] Y. Wang, X. Wang, Y. Qin, L. Zhang, and Y. Wang, "Three-dimensional numerical study of a cathode gas diffusion layer with a through/in plane synergetic gradient porosity distribution for PEM fuel cells," *Int. J. Heat Mass Transf.*, vol. 188, Jun. 2022, Art. no. 122661.

[21] Y. Wang, H. Xu, Z. Zhang, H. Li, and X. Wang, "Lattice Boltzmann simulation of a gas diffusion layer with a gradient polytetrafluoroethylene distribution for a proton exchange membrane fuel cell," *Appl. Energy*, vol. 320, Aug. 2022, Art. no. 119248.

[22] L. Xu and J. Xiao, "Modeling and simulation of the dynamic behavior of proton exchange membrane fuel cell," *J. WUT*, vol. 29, pp. 10–13, Jan. 2007.

[23] L. Xu and J. Xiao, "Modeling and simulation of PEM fuel cells based on electrochemical model," in *Proc. Int. Conf. Remote Sens., Environ. Transp. Eng.*, Jun. 2011, pp. 471–474.

[24] J. M. Correa, F. A. Farret, L. N. Canha, and M. G. Simoes, "An electrochemical-based fuel-cell model suitable for electrical engineering automation approach," *IEEE Trans. Ind. Electron.*, vol. 51, no. 5, pp. 1103–1112, Oct. 2004.

[25] H. Lohse-Busch, K. Stutenberg, M. Duoba, X. Liu, A. Elgowainy, M. Wang, T. Wallner, B. Richard, and M. Christenson, "Automotive fuel cell stack and system efficiency and fuel consumption based on vehicle testing on a chassis dynamometer at minus 18 °C to positive 35 °C temperatures," *Int. J. Hydrogen Energy*, vol. 45, no. 1, pp. 861–872, Jan. 2020.

[26] D. Zhou, A. Al-Durra, I. Matraji, A. Ravey, and F. Gao, "Online energy management strategy of fuel cell hybrid electric vehicles: A fractional-order extremum seeking method," *IEEE Trans. Ind. Electron.*, vol. 65, no. 8, pp. 6787–6799, Aug. 2018.

[27] G. Giordano, V. Klass, M. Behm, G. Lindbergh, and J. Sjöberg, "Model-based lithium-ion battery resistance estimation from electric vehicle operating data," *IEEE Trans. Veh. Technol.*, vol. 67, no. 5, pp. 3720–3728, May 2018.

[28] W. Niu, K. Song, Y. Zhang, Q. Xiao, M. Behrendt, A. Albers, and T. Zhang, "Influence and optimization of packet loss on the internet-based geographically distributed test platform for fuel cell electric vehicle powertrain systems," *IEEE Access*, vol. 8, pp. 20708–20716, 2020.

[29] J. J. E. Slotine and W. Li, *Applied Nonlinear Control*. Englewood Cliffs, NJ, USA: Prentice-Hall, 1991.

[30] F. M. Asl and A. G. Ulsoy, "Analysis of a system of linear delay differential equations," *J. Dyn. Syst., Meas., Control*, vol. 125, no. 2, pp. 215–223, 2003.

[31] X. Ge, M. J. Brudnak, P. Jayakumar, J. L. Stein, and T. Ersal, "A model-free predictor framework for tele-operated vehicles," in *Proc. Amer. Control Conf. (ACC)*, Chicago, IL, USA, Jul. 2015, pp. 4573–4578.

WENXU NIU was born in Henan, China, in 1990. She received the bachelor's and Ph.D. degrees in automotive engineering from Tongji University, Shanghai, China, in 2014 and 2019, respectively.

Since 2013, she has been a Research Assistant with the Institute of Fuel Cell Vehicle Technology, Tongji University. Since 2019, she has been an Assistant Professor with the School of Intelligent Manufacturing and Control Engineering, Shanghai Polytechnic University. Her research interests include automotive powertrain system distributed test validation, transmission analysis, and transmission optimization method.

CAIPING LIANG was born in Shanxi, China, in 1977. She received the Ph.D. degree in mechanical engineering from Shanghai Jiao Tong University, in 2008.

Since 2008, she has been an Assistant Professor with the Department of Mechanical Engineering, Shanghai Polytechnic University, China. She is the author of 20 articles and more than ten inventions. Her research interests include automobile body quality control, automobile product development, and intelligent networked automobile.